Energies **2014**, *7*, 6172-6185; doi:10.3390/en7096172

OPEN ACCESS

energies

ISSN 1996-1073

www.mdpi.com/journal/energies

Article

Experimental Investigation of the Performance of a Hermetic Screw-Expander Organic Rankine Cycle

Sung-Wei Hsu [1,*], Hsiao-Wei D. Chiang [2] and Chih-Wei Yen [1]

[1] Green Energy Research Laboratories, Industrial Technology Research Institute, Hsinchu 310, Taiwan; E-Mail: cwyen@itri.org.tw

[2] Department of Power Mechanical Engineering, National Tsing Hua University, Hsinchu 300, Taiwan; E-Mail: hwchiang@mx.nthu.edu.tw

* Author to whom correspondence should be addressed; E-Mail: rosetty@itri.org.tw; Tel.: +886-3-591-5392; Fax: +886-3-582-0017.

Received: 6 June 2014; in revised form: 15 August 2014 / Accepted: 22 September 2014 / Published: 23 September 2014

Abstract: In this study, the authors experimentally investigate the performance of the organic Rankine cycle (ORC) and screw expander under the influence of supply pressure and pressure ratio over the expander. Three tests were performed with expander pressure ratios of 2.4–3.5, 3.0–4.6, and 3.3–6.1, which cover the over-expansion and under-expansion operating modes. The test results show a maximum expander isentropic efficiency of 72.4% and a relative cycle efficiency of 10.5% at an evaporation temperature of 101 °C and condensation temperature of 45 °C. At a given pressure ratio over the expander, a higher supply pressure to the expander causes a higher expander isentropic efficiency and higher cycle efficiency in the over-expansion mode. However, in the under-expansion mode, the higher supply pressure results in a lower expander isentropic efficiency and adversely affects the cycle efficiency. The results also show that under the condition of operation at a given pressure ratio, a higher supply pressure yields a larger power output owing to the increased mass flow rate at the higher supply pressure. The study results demonstrate that a screw-expander ORC can be operated with a wide range of heat sources and heat sinks with satisfactory cycle efficiency.

Keywords: organic Rankine cycle; hermetic oil-lubricated twin-screw expander; expander expansion ratio; expander isentropic efficiency; cycle electricity efficiency

---

1. Introduction

The approach of burning fossil fuels to obtain heat for use in thermal processes or power for mechanical drivers has been employed for centuries. However, this burning process produces carbon dioxide, which is a greenhouse gas and is harmful to the environment as it contributes to problems such as air pollution, global warming, and climate change. Reserves of fossil fuels such as oil, coal, and gas are predicted to be depleted within approximately 35, 107, and 37 years, respectively [1]. As a consequence, the prices of oil and gas will increase continually and more drastically through these years. In order to resolve these problems, *i.e.*, to mitigate greenhouse gas emissions and fossil fuel depletion, much effort has been made toward using industrial waste heat and renewable energies for producing electricity.

A variety of low-grade heat sources, such as flue gas, hot water produced during thermal processes, and waste steam, are rejected to the environment because they have comparatively low energy availability and are not very economical. The rejection of low-grade heat sources accounts for 30%–50% of the total energy loss in industries. The recovery and exploitation of such lost energies of low-grade heat sources have then attracted considerable attention from the viewpoint of reducing greenhouse gas emissions and improving energy usage efficiency. Among the available energy recovery methods, the organic Rankine cycle (ORC), which employs low-boiling-point organic fluids, is regarded as one of the most promising candidates because of its simplicity and superior thermal efficiency [2].

Many studies have been conducted on ORC systems in the past decade; these studies focused on aspects such as optimization of cycle efficiency [3–5], selection of working fluids [6–8], economic design of the ORC system [2,9], proof-of-concept demonstrations [10,11], application of waste heat [12–14], geothermal power systems [15,16], and utilization of solar energy [17,18]. Results of the aforementioned studies have shown that the key components of an ORC system, such as heat exchangers and expanders, have a significant influence on the system performance. The isentropic efficiency of the expander and the exergy losses of the evaporator and condenser [19] are considered as the most critical factors for optimizing the performance of an ORC system. Effects of degree of superheat at expander inlet was studied with different evaporator type in an ORC system with pure substance as working fluid [20] and an optimum superheat of 40K was explored for an ORC system with mixture R416A as working fluid applied to the waste heat recovery from the diesel engine exhaust [21].

Power-generating devices used for the ORC can be categorized into volumetric devices [22] (such as reciprocating piston-cylinder devices, scroll expanders [23,24], screw expanders [25,26], and rotary displacement machines) and dynamic devices (such as axial flow turbines [27] and radial inflow turbines [28]). Lemort *et al.* [23] and Quoilin *et al.* [24] used a scroll expander as an ORC core engine and revealed that the isentropic efficiency of the scroll expander was affected mainly by the pressure ratios across the expander. Among the above-listed expanders, screw expanders were proposed to be candidates for 10–300-kW ORCs. In these studies, it was revealed that the isentropic efficiency of a scroll expander is affected mainly by the pressure ratio over the screw expander, and there exists an optimum expander isentropic efficiency [23,24]. However, another study shows that the relation between inlet pressure and isentropic efficiency is more complicated [29]. The present study attempts

to investigate the influence of the supply pressure and pressure ratio on the performance of both the screw expander and the ORC system. A 50-kW ORC system was designed and constructed, using an oil-injected twin-screw expander as the engine core and R245fa as the working fluid. Three tests were performed, in which the expander pressure ratios were set to 3.3–6.1, 3.0–4.6, and 2.4–3.5 to investigate their effects on the expander performance, system cycle efficiency, and power output.

2. System Description

A 50-kW ORC, with R245fa as the working fluid, was designed and constructed to convert hot water heat energy (80–125 °C) into electricity. The schematic diagram of this 50-kW ORC system is shown in Figure 1. The main components of this system are a multistage centrifugal pump, a plate-type evaporator, an oil-injected twin-screw expander integrated with an induction generator, an oil separator, an oil pump, and a shell-and-tube-type condenser. Temperature and pressure transducers are arranged at the inlet and outlet of each component. A pickup sensor (logic magnetic pickups) was installed to measure the rotational speed of the generator. A vortex flowmeter was installed at the outlet of the centrifugal pump to measure the flow rate of R245fa, and a multipower meter was used to measure the electricity output, which includes the voltage, current, power, and power factor. The flow rate of R245fa was automatically regulated by the pump, which was controlled by a variable-frequency inverter. The installation positions of these components are indicated in Figure 1. Table 1 lists the sensor types and their accuracies.

Figure 1. Schematic diagram of 50-kW ORC system used in this study.

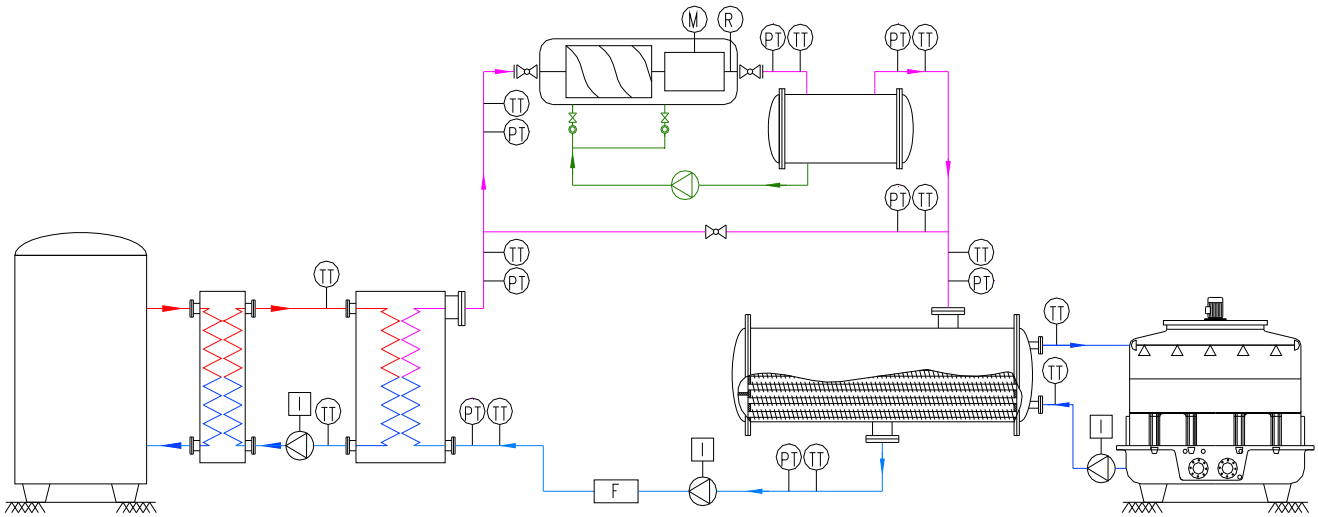

Table 1. Types and accuracies of sensors used in this study.

Sensor	Type	Accuracy
Pressure transducer	Piezoelectric type	±1.0% of 2500 kPa
Temperature transducer	RTD Pt100 (3 wires)	±0.25 °C
Water flowmeter	Electromagnetic type	±1.0%
Liquid R245fa flowmeter	Vortex type	±0.7%
Electric power meter	Multipower meter	±0.1%

The screw expander used in this ORC system was a hermetic oil-injected twin-screw expander. The rotor of the expander was directly integrated into the rotating shaft of the induction generator. The rotational speed of the generator ranges from 3610 rpm to 3670 rpm. The nominal volumetric flow rate of the expander is 410 m^3/h, and its built-in volume ratio is 4.8 (Figure 2). Figure 3 shows the three-dimensional (3-D) layout and photograph of the 50-kW ORC unit.

Figure 2. Configuration of a hermetic twin-screw expander integrated with an induction generator.

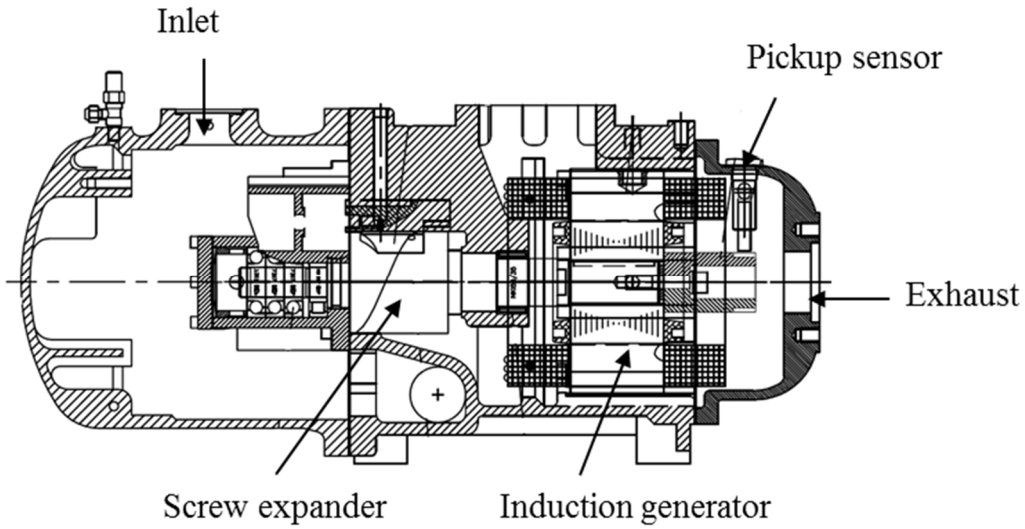

Figure 3. Three-dimensional layout (**left**) and photograph (**right**) of the ORC unit.

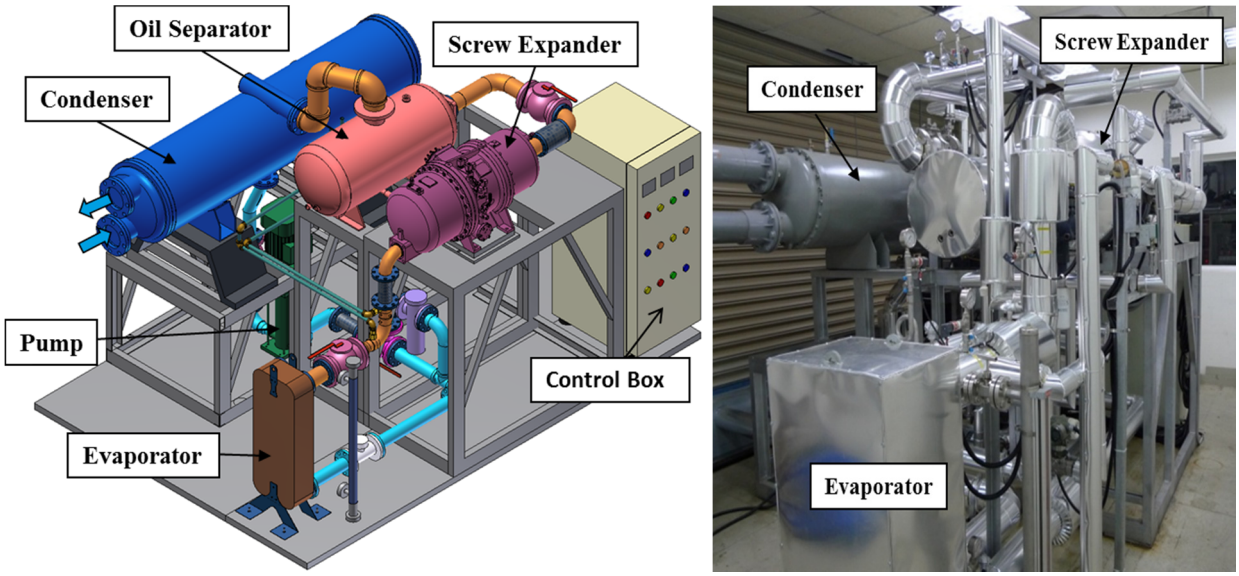

A boiler with a heat capacity of 1050 kW was employed as the heat supply system. The steam generated by the boiler heated high-pressure water to a temperature of 80–125 °C via a plate-type heat exchanger. Then, hot water was supplied to the water side of the ORC evaporator, where R245fa was heated, evaporated and superheated. A 200-RT cooling tower was used as the heat rejection system for the ORC. The coolant water was pumped into the water side of the ORC condenser to condense the superheated R245fa into liquid. The design point of the 50-kW ORC system was set to an evaporation temperature of 105 °C (evaporation pressure of 1.411 MPa) and a condensation temperature of 40 °C

(condensation pressure of 0.250 MPa). The overall efficiency of the pumping system (pump and motor) was 59.8%, the isentropic efficiency of the expander was 75%, and the efficiency of the generator was 92%. A superheated temperature level of 15 °C was set for the vapor working fluid (R245fa) before it entered the expander. The REFPROP 9.0 software was used to calculate the fluid properties. At the design point, the predicted gross power was 50 kW with a cycle efficiency of 9.46%. The volumetric expansion ratio of the expander at the design point was 5.94, and the relative pressure ratio over the expander was 5.5.

To determine the effects of the supply pressures on the expander, and the pressure ratios over it on the performances of both the screw expander and the ORC cycle, the following three tests were intentionally performed by regulating the heat input and heat rejection:

(1) Test 1: The temperature of the hot water was regulated to be in the range of 85–122 °C and the flow rate of the coolant water was fixed at 400 LPM (liters per minute). During this test, the cooling fan of the cooling tower was turned off to lower its heat rejection capacity.
(2) Test 2: The temperature of the hot water was regulated to be in the range of 90–122 °C and the flow rate of the coolant water was fixed at 300 LPM. During this test, the cooling fan of the cooling tower was turned on.
(3) Test 3: The temperature of the hot water was regulated to be in the range of 80–118 °C and the flow rate of the coolant water was fixed at 1200 LPM. During this test, the cooling fan of the cooling tower was turned on.

All three tests were performed under a fixed hot-water flow rate of 450 LPM. For each test, the temperature level of the hot water was regulated to achieve the heat input level required by the ORC evaporator. To maintain the superheated temperature level of 15 °C at the expander inlet, the pump speed was regulated by automatically controlling the evaporation pressure of R245fa by using an inverter. The inlet and outlet temperatures of the cold water were related to the ambient temperature, coolant water flow rate, cooling fan, and heat rejection of the ORC system. Table 2 presents the conditions of the hot water and coolant water in the three tests.

The main difference among the three tests is the design of heat rejection. For a specific hot water temperature, a lower mass flow rate of coolant water will result in a higher condensation temperature in the ORC system. In Test 3, the coolant water flow rate is higher than the other two, so that the condensation temperature will be lower than the other two. In Test 1, the coolant water flow rate is 400 LPM, which is a little higher than that in Test 2. However, the cooling fan is turn off in Test 1, while the cooling fan is turn on in Test 2. This arrangement will result in a higher condensation temperature in Test 1 than in Test 2.

The large range for hot water temperature was designed to get different evaporation temperatures. The temperature of coolant water was varied with hot water temperature. For instance in Test 2, the initial temperature of hot water is 90 °C and the inlet temperature of coolant water is 24 °C, resulted in a evaporation temperature of 74.5 °C and a condensation temperature of 36.3 °C. Then, the hot water temperature was adjusted to 100 °C manually, the evaporation temperature was automatically increased to 84.3 °C, and condensation temperature increased to 38.4 °C because of the higher mass flow rate, and the outlet temperature of coolant water was increased to 37.4 °C due to the higher mass flow rate.

Table 2. Conditions of hot water and coolant water used in the three tests.

Conditions		Mass flow rate (LPM)	Inlet temperature (°C)	Outlet temperature (°C)
Test 1	Hot water	~450	85–122	74–101
	Coolant water	~400	32–39	39–55
Test 2	Hot water	~450	90–122	78–101
	Coolant water	~300	24–26	36–46
Test 3	Hot water	~450	80–118	70–96
	Coolant water	~1200	22–26	25–31

3. Theoretical Modeling

Volumetric expanders are characterized by a built-in volume ratio, which is defined as the volumetric expansion rate of the fluid trapped in the closed pocket during the expansion process. Some studies compared the effect of a mismatch between the volume ratio over the expander and its built-in volume ratio, for both a scroll expander and a screw expander [9,10]. In the "under-expansion mode" considered in these studies, the volume ratio over the expander is higher than its built-in volume ratio. The pressure P_{int} in the expansion chambers at the end of the expansion process is higher than the pressure P_{ex} at the expander exhaust. In contrast, in the "over-expansion mode", the volume ratio over the expander is lower than its built-in volume ratio. In this mode, the pressure P_{int} is lower than the pressure P_{ex}.

The work done by an expander in the under- and over-expansion operating modes can be modeled by splitting the expansion process into two sub-processes [9]: isentropic expansion ($W_1 = h_{expd,su} - h_{expd,int,s}$) and constant-volume expansion ($W_2 = V_{int}(P_{int} - P_{ex})$). The constant-volume-expansion work (W_2) is positive in the under-expansion mode but negative in the over-expansion mode.

The isentropic efficiency of the expander, η_{expd}, was calculated for all test data. This efficiency is defined as the ratio of the enthalpy drop (derived from the measured temperature and pressure) to the isentropic enthalpy drop during the expansion process.

$$\eta_{expd} = \frac{(h_{expd,su} - h_{expd,ex})}{(h_{expd,su} - h_{expd,ex,s})} \quad (1)$$

ORC is used for heat energy conversion, the evaporation pressure and condensation pressure of circulating working fluid will change to meet the condition of heat source and heat sink. This implies that the pressure ratio over the expander (PI), defined as the ratio of the supply pressure (P_{su}) at expander inlet and exhaust pressure (P_{ex}) at expander exhaust, is not a fixed value. To investigate the effects of the pressure ratio (PI) over the expander on the isentropic efficiency of the expander, the expander performance was modeled with condensation temperatures (T_{cond}) of 20 °C, 30 °C, and 40 °C. The isentropic efficiency loss due to the internal leakage of the expander was set as 20%. Other minor losses (such as heat transfer, mechanical loss, and pressure loss) were assumed to be 8%. Figure 4 shows the expander isentropic efficiency η_{expd} as a function of PI values of 3–10 and various supply pressures. The maximum isentropic efficiency is attained when PI equals $PI_{built\text{-}in}$. For each value of T_{cond}, η_{expd} decreased sharply with decreasing PI in the over-expansion operating mode, whereas it decreased only slightly with increasing PI in the under-expansion operating mode.

Figure 4. Modeled effects of PI and supply pressure on expander isentropic efficiency.

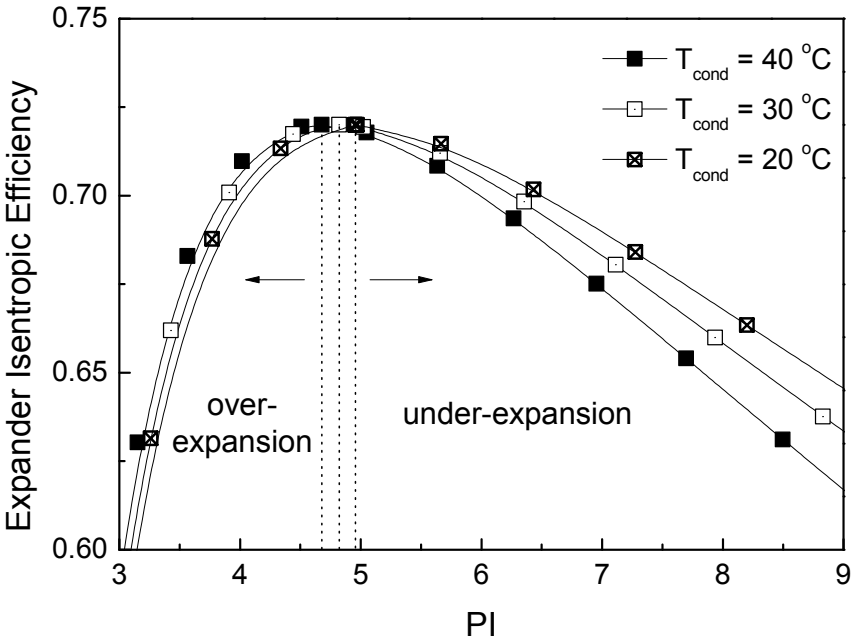

At a fixed PI, a higher T_{cond} corresponds to a higher exhaust pressure (P_{ex}) and a higher supply pressure (P_{su}). The result shows that the influence of supply pressure on the isentropic efficiency of the screw expander in the over-expansion mode is quite different from that in the under-expansion mode. It can be observed in Figure 4 that the values of η_{expd} for a T_{cond} of 40 °C (corresponding to the highest supply pressure) is higher than those for a T_{cond} of 30 °C and 20 °C in the over-expansion operating mode, whereas the values of η_{expd} for a T_{cond} of 40 °C is lower than those for a T_{cond} of 30 °C and 20 °C in the under-expansion mode. It should be noted that the influence of the supply pressure on η_{expd} becomes stronger when PI is much higher than the built-in PI.

4. Results and Discussion

Figure 5a shows the plot of the evaporation temperature T_{evap} *versus* the condensation temperature T_{cond}. Figure 5b shows the plot of the relative evaporation pressure P_{evap} *versus* the condensation pressure P_{cond}. As shown in Figure 5a,b, for a fixed T_{evap}, the lowest T_{cond} and P_{cond} occur in Test 3 because the coolant-water flow rate is the highest in this test (1200 LPM). On the other hand, the highest T_{cond} and P_{cond} occur in Test 1 because this test has the lowest heat rejection capacity because the cooling fan is turned off.

Based on the test data shown in Figure 5, Figure 6 shows the relationship of the pressure ratios (PI) with the volume ratios (VI) for each test. The PI values over the expander in these three tests are in the range of 2.4–3.5 (Test 1), 3.0–4.6 (Test 2), and 3.3–6.1 (Test 3), covering both the over-expansion and the under-expansion operating modes. At a certain VI value, for example, VI = 3.81, the PI value in Test 3 is 3.72, which is higher than that in Test 2 (PI = 3.66) and Test 1 (PI = 3.52). This is because the P_{cond} in Test 3 is the lowest among that in the three tests and the P_{cond} in Test 1 is the highest.

Figure 5. Plots of (**a**) T_{cond} *vs*. T_{evap} and (**b**) P_{cond} *vs*. P_{evap} for the three tests.

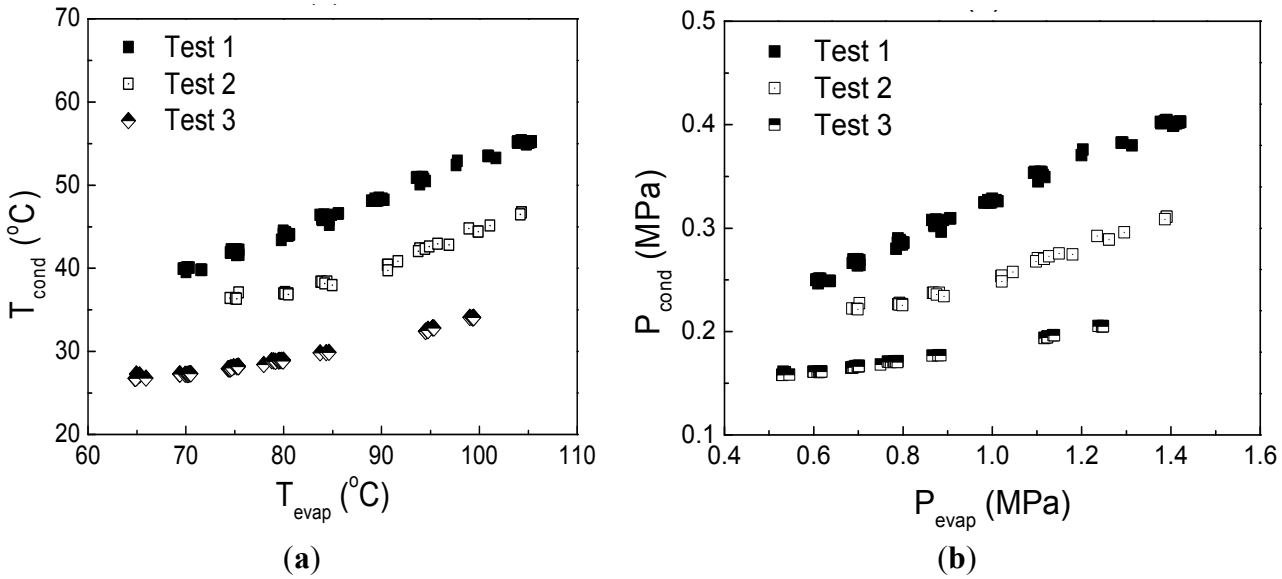

Figure 6. Variation in PI with changing VI for each test.

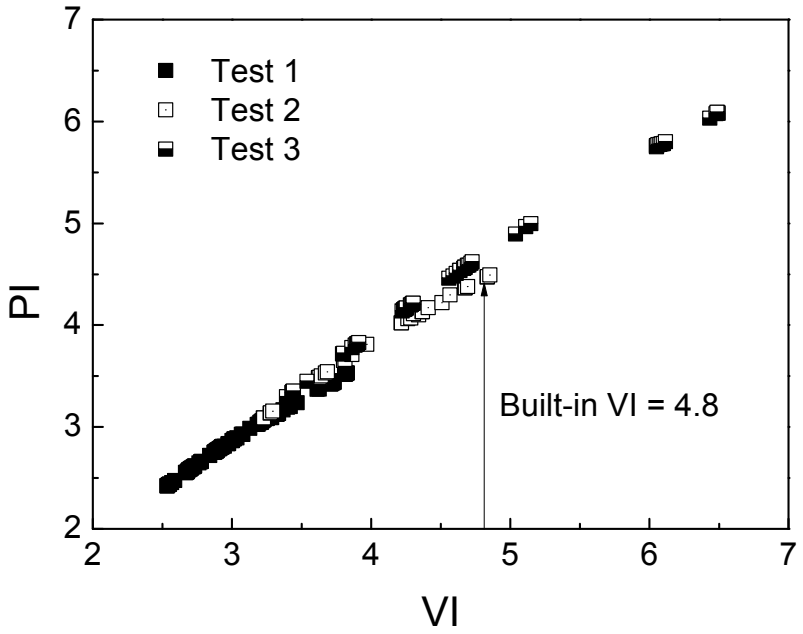

Figure 7 shows the expander isentropic efficiency η_{expd} as a function of PI in all three tests. The data of Test 1 and Test 2 lie in the region of the over-expansion mode, whereas those of Test 3 are spread over both the over-expansion mode and the under-expansion mode.

For all three tests, η_{expd} increases with increasing PI in the over-expansion mode. The maximum η_{expd} values in Test 1, Test 2, and Test 3 are 71.8%, 72.4%, and 72.5%, respectively. The corresponding PI values for Test 1, Test 2, and Test 3 are 3.5 (VI = 3.8), 4.4 (VI = 4.7), and 5.7 (VI = 6.0), respectively. In Test 3, the PI with maximum η_{expd} is slightly higher than $PI_{built\text{-}in}$ ($PI_{built\text{-}in}$ is 4.7 for Test 3), which implies that the screw expander exhibits optimum performance in the under-expansion mode. This is different from the result shown in Figure 4 wherein the maximum η_{expd} is theoretically located at PI = $PI_{built\text{-}in}$; it in fact occurs at a higher PI due to the influence of the supply

pressure drop, friction, and irreversibility of flow inside the expander. After η_{expd} attains the maximum value, it decreases slightly with increasing PI. According to this result, it is recommended that the $PI_{built\text{-}in}$ of the screw expander be set slightly lower than the pressure ratio over the screw expander when designing an ORC system. This will offer two advantages: (1) the optimum expander isentropic efficiency can be achieved at the design point and (2) a significant drop in η_{expd} in the over-expansion mode can be avoided.

Figure 7. Test results of effects of PI and supply pressure on expander isentropic efficiency.

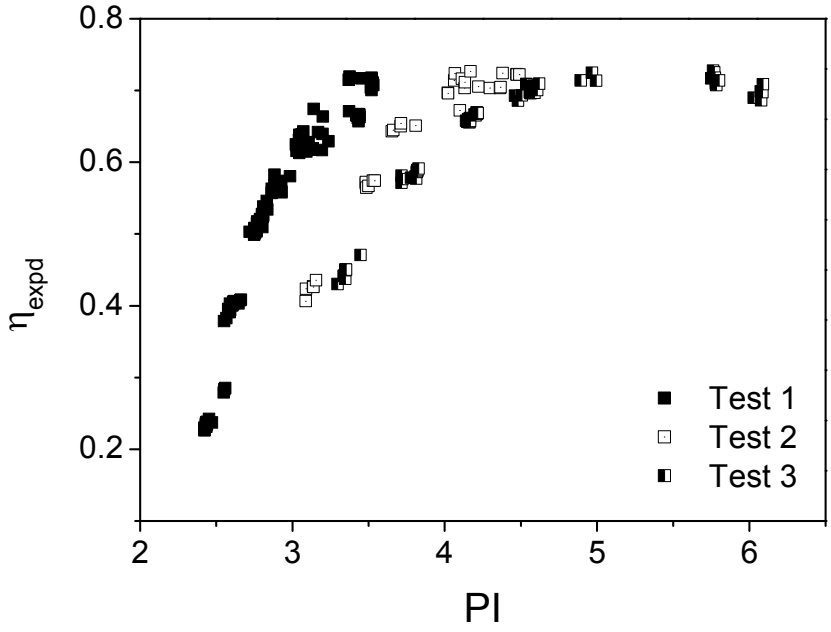

Figure 7 also shows that the η_{expd} of Test 1 is higher than those of Test 2 and Test 3 at a given PI. This result can be explained by the fact that the supply pressure is highest in Test 1 among the three tests; this result is consistent with the modeling result shown in Figure 6.

Figure 8 shows the measured electrical power as a function of PI. The maximum electrical power of 50 kW was achieved at PI = 6.08 in Test 3, with T_{evap} = 99.4 °C and T_{cond} = 34 °C. The corresponding η_{expd} is 68.62%, which is lower than the maximum value. For a fixed PI, the power outputs for the three tests are rather different. As shown in Table 3, for PI = 3.4, the electrical power output in Test 1 is two times that in Test 2 and four times that in Test 3. This result is attributed to the larger temperature difference, higher expander isentropic efficiency, and higher mass flow rate in Test 1 as compared to those in Test 2 and Test 3. An important characteristic of a positive-displacement expander is the swept volume. The swept volume is fixed for a given screw expander. Therefore, a higher supply pressure will correspond to a higher supply density of the working fluid and will allow a larger amount of R245fa to pass through the expander, which will in turn lead to a larger power output at a constant PI.

Figure 8. Effects of PI and supply pressure on electrical power output.

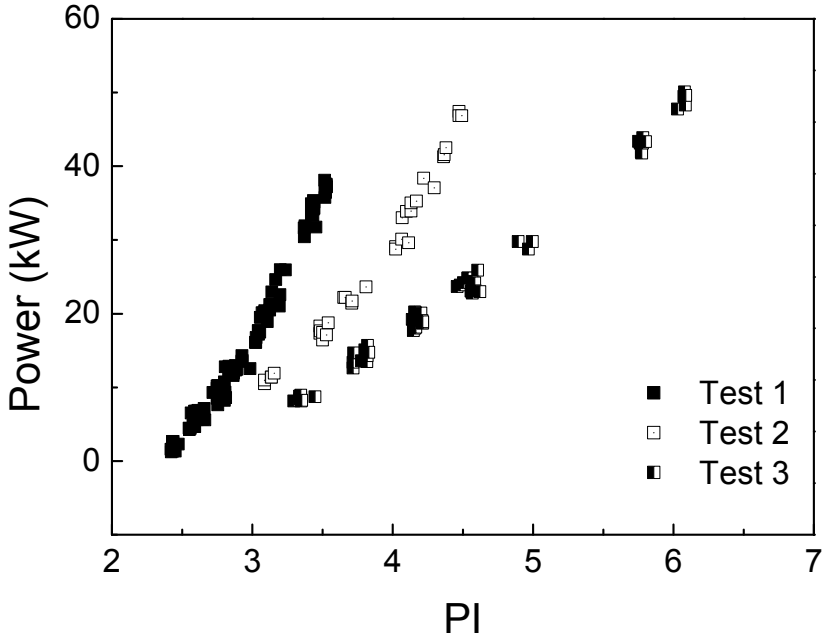

Table 3. Operation conditions for the three tests at system PI ≈ 3.4.

Operation conditions	Test 1	Test 2	Test 3
T_{evap}, °C	104.2	80.4	65.9
T_{cond}, °C	55.2	37.2	26.8
ΔP over the expander, kPa	983.5	569.8	387.43
Power, kW	34.26	16.8	8.73
η_{cycle}	6.95%	6.03%	4.23%

Figure 9 shows the cycle efficiency η_{cycle} as a function of PI. η_{cycle} is defined as the electricity output of the cycle divided by the measured heat input to the working fluid. This efficiency can be affected by the supply pressure (P_{su}), pressure difference (ΔP), expander isentropic efficiency (η_{expd}), and alternator efficiency (η_{alt}) as follows.

$$\eta_{cycle} = \frac{P_{elect}}{\dot{Q}_{evap}} = \frac{\dot{M}_{wf}(h_{expd,su} - h_{expd,ex,s}) \times \eta_{expd} \times \eta_{alt}}{\dot{M}_{wf} \times (h_{expd,su} - h_{pumd,ex})} = \frac{(h_{expd,su} - h_{expd,ex,s})}{(h_{expd,su} - h_{pump,ex})} \times \eta_{expd} \times \eta_{alt} \quad (2)$$

Among the three tests, at a given PI, the η_{cycle} value is highest for Test 1. This can be illustrated by the fact that both P_{su} and ΔP over the expander for Test 1 are higher than those for Test 2 and Test 3, which gives a higher value of $(h_{expd,su} - h_{expd,ex,s})/(h_{expd,su} - h_{pump,ex})$ and correspondingly a higher value of η_{cycle}. Furthermore, the higher P_{su} in the over-expansion mode is expected to provide an extra gain in η_{expd}. On the other hand, in the under-expansion mode, the lower η_{expd} corresponding to higher P_{su} is expected to reduce η_{cycle}, according to the modeling result in Figure 4.

Figure 9. Effects of PI and supply pressure on cycle efficiency.

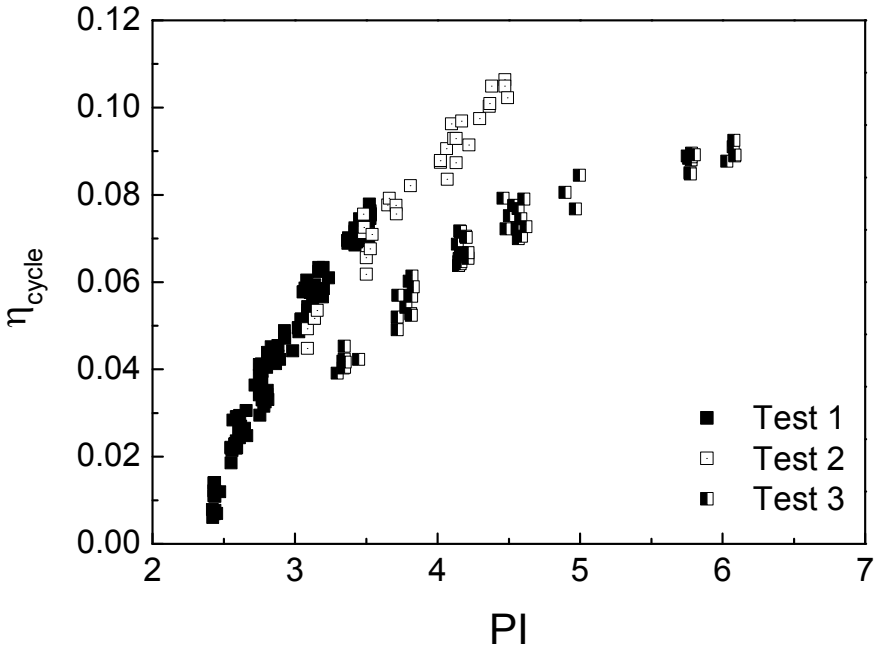

5. Summary and Conclusions

This experimental study investigated the performance of a 50-kW screw-expander ORC system under the influence of varying supply pressures and pressure ratios. Three tests with different coolant-water flow rates were conducted for expansion pressure ratios of 2.4–3.5, 3.0–4.6, and 3.3–6.1. The effects of different supply pressures on the performances of the screw expander and ORC system were reported. Based on the foregoing discussions, the following conclusions can be made.

(1) The isentropic efficiency of a screw expander reaches its maximum value at a PI that is slightly higher than its built-in PI. In the over-expansion mode, the isentropic efficiency drops rapidly with decreasing PI, but in the under-expansion mode, it drops only slightly with increasing PI. It is then recommended to set the built-in volume ratio of the screw expander slightly lower than the system VI to avoid operation in the over-expansion mode.

(2) At constant pressure ratios, a higher supply pressure results in a higher isentropic efficiency of the expander and a higher cycle efficiency during the over-expansion operating mode. However, such a pressure will induce a lower isentropic efficiency of the expander in the under-expansion operating mode.

(3) The cycle efficiency of the ORC system is affected by the expander isentropic efficiency and the difference between the evaporation temperature and the condensation temperature. At a given PI, a higher supply pressure implies a larger temperature difference and results in a higher cycle efficiency. In the over-expansion operating mode, a higher supply pressure is beneficial because it implies a comparatively higher isentropic efficiency of the expander, which in turn will result in an increase in the cycle efficiency. However, in the under-expansion operating mode, a higher supply pressure will reduce the system cycle efficiency.

(4) The power output of the ORC system is determined mainly by the mass flow rate of the working fluid and the cycle efficiency. The influence of the expander isentropic efficiency on

the power output is minor. For a higher supply pressure at a given PI, a larger amount of superheated R245fa vapor is allowed to pass through the expander. Moreover, the corresponding higher expander isentropic efficiency and cycle efficiency altogether will result in a higher power output, as demonstrated through the test results.

Acknowledgments

The authors would like to express their sincere gratitude for the Energy R&D foundation funding from the Bureau of Energy of the Ministry of Economic Affairs of Taiwan ROC.

Author Contributions

Sung-Wei Hsu designed the ORC system, built the theoretical model of the screw expander and ORC, performed the simulations, and analyzed the experimental data. Chih-Wei Yen conceptualized and set up the ORC system. Hsiao-Wei D. Chiang verified the results and the entire manuscript.

Nomenclature

$h_{expd,ex}$	specific enthalpy at expander exhaust, kJ/kg
$h_{expd,ex,s}$	specific isentropic enthalpy at expander exhaust, kJ/kg
$h_{expd,su}$	specific enthalpy at expander inlet, kJ/kg
$h_{expd,int,s}$	specific isentropic enthalpy at the end of internal expansion, kJ/kg
$h_{pump,ex}$	specific enthalpy at pump exhaust, kJ/kg
P_{cond}	condensation pressure of ORC cycle, kPa
P_{evap}	evaporation pressure of ORC cycle, kPa
P_{ex}	exhaust pressure at expander exhaust, kPa
P_{su}	supply pressure at expander inlet, kPa
P_{int}	internal pressure at the end of the expansion process inside expander, kPa
PI	pressure ratio over expander, P_{su}/P_{ex}
$PI_{built\text{-}in}$	built-in pressure ratio of expander, P_{su}/P_{int}
P_{elect}	measured electricity output, kW
Q_{evap}	heat transfer rate in evaporator, kW
T_{cond}	condensation temperature of ORC cycle, °C
T_{evap}	evaporation temperature of ORC cycle, °C
VI	volume ratio over expander, v_{ex}/v_{su}
$VI_{built\text{-}in}$	built-in volume ratio of expander, v_{ex}/v_{int}
V_{int}	internal volume flow rate of expander, m^3/s
W_1	expansion work for isentropic expansion process, kW
W_2	expansion work for constant-volume expansion process, kW
η_{expd}	isentropic efficiency of twin-screw expander
η_{alt}	electrical efficiency of alternator
η_{pump}	isentropic efficiency of multistage centrifugal pump
η_{cycle}	cycle efficiency of ORC

Conflicts of Interest

The authors declare no conflict of interest.

References

1. Shahriar, S.; Erkan, T. When will fossil fuel reserves be diminished? *Energy Policy* **2009**, *37*, 181–189.
2. Schuster, A.; Karellas, S.; Kakaras, E.; Spliethoff, H. Energetic and economic investigation of organic Rankine cycle applications. *Appl. Therm. Eng.* **2009**, *29*, 1809–1817.
3. Wei, D.; Lu, X.; Lu, Z.; Gu, J. Performance analysis and optimization of organic Rankine cycle (ORC) for waste heat recovery. *Energy Convers. Manag.* **2007**, *48*, 1113–1119.
4. Dai, Y.; Wang, J.; Gao, L. Parametric optimization and comparative study of organic Rankine cycle (ORC) for low grade waste heat recovery. *Energy Convers. Manage.* **2009**, *50*, 576–582.
5. Zhang, S.; Wang, H.; Guo, T. Performance comparison and parametric optimization of subcritical organic Rankine cycle (ORC) and transcritical power cycle system for low-temperature geothermal power generation. *Appl. Energy* **2011**, *88*, 2740–2754.
6. Saleh, B.; Koglbauer, G.; Wendland, M.; Fischer, J. Working fluids for low-temperature organic Rankine cycles. *Energy* **2007**, *32*, 1210–1221.
7. Tchanche, B.F.; Papadakis, G.; Lambrinos, G.; Frangoudakis, A. Fluid selection for a low-temperature solar organic Rankine cycle. *Appl. Therm. Eng.* **2009**, *29*, 2468–2476.
8. Abbin, J.P.; Leuenberger, W.R. *Program CYCLE: A Rankine Cycle Analysis Routine*; Sandia National Laboratories Report SAND 74–0099 (revised); Sandia Laboratories: Albuquerque, NM, USA, 1974.
9. Quoilin, S.; Declaye, S.; Tchanche, B.F.; Lemort, V. Thermo-economic optimization of waste heat recovery organic Rankine cycles. *Appl. Therm. Eng.* **2011**, *31*, 2885–2893.
10. Aghahosseini, S.; Dincer, I. Comparative performance analysis of low-temperature organic Rankine cycle (ORC) using pure and zeotropic working fluids. *Appl. Therm. Eng.* **2013**, *54*, 35–42.
11. Garg, P.; Kumar, P.; Srinivasan, K.; Dutta, P. Evaluation of carbon dioxide blends with isopentane and propane as working fluids for organic Rankine cycles. *Appl. Therm. Eng.* **2013**, *52*, 439–448.
12. Liu, B.; Chien, K.; Wang, C.C. Effect of working fluids on organic Rankine cycle for waste heat recovery. *Energy* **2004**, *29*, 1207–1217.
13. Schroeder, D.J.; Leslie, N. Organic Rankine cycle working fluid considerations for waste heat to power applications. *ASHRAE Trans.* **2010**, *116*, 525–532.
14. Larjola, J. Electricity from industrial waste heat using high-speed organic Rankine cycle (ORC). *Int. J. Prod. Econ.* **1995**, *41*, 227–235.
15. Hettiarachchi, M.H.D.; Golubovic, M.; Worek, W.M.; Ikegami, Y. Optimum design criteria for an organic Rankine cycle using low-temperature geothermal heat sources. *Energy* **2007**, *32*, 1698–1706.

16. Borsukiewicz-Gozdur, A.; Nowak, W. Maximising the working fluid flow as a way of increasing power output of geothermal power plant. *Appl. Therm. Eng.* **2007**, *27*, 2074–2078.
17. Wang, X.D.; Zhao, L.; Wang, J.L.; Zhang, W.Z.; Zhao, X.Z.; Wu, W. Performance evaluation of a low-temperature solar Rankine cycle system utilizing R245fa. *Solar Energy* **2010**, *84*, 353–364.
18. Li, J.; Pei, G.; Ji, J. Optimization of low temperature solar thermal electric generation with organic Rankine cycle in different areas. *Appl. Energy* **2010**, *87*, 3355–3365.
19. Li, J.; Pei, G.; Li, Y.; Wang, D.; Ji, J. Energetic and exergetic investigation of an organic Rankine cycle at different heat source temperatures. *Energy* **2012**, *38*, 85–95.
20. Lee, Y.R.; Kuo, C.R.; Liu, C.H.; Fu, B.R.; Hsieh, J.C.; Wang, C.C. Dynamic Response of a 50 kW organic Rankine cycle system in association with evaporators. *Energies* **2014**, *7*, 2436–2448.
21. Yang, K.; Zhang, H.; Song, S.; Yang, F.; Liu, H.; Zhao, G.; Zhang, J.; Yao, B. Effects of degree of superheat on the running performance of an organic Rankine cycle (ORC) wasted heat recovery system for diesel engines under various operating conditions. *Energies* **2014**, *7*, 2123–2145.
22. Quoilin, S.; Declaye, S.; Lemort, V. Expansion machine and fluid selection for the organic rankine cycle. In Proceedings of the 7th International Conference on Heat Transfer, Fluid Mechanics and Thermodynamics (HEFAT2010), Antalya, Turkey, 19–21 July 2010.
23. Lemort, V.; Quoilin, S.; Cuevas, C.; Lebrun, J. Testing and modeling a scroll expander integrated into an organic Rankine cycle. *Appl. Therm. Eng.* **2009**, *29*, 3094–3102.
24. Quoilin, S.; Lemort, V.; Lebrun, J. Experimental study and modeling of an organic Rankine cycle using scroll expander. *Appl. Energy* **2010**, *87*, 1260–1268.
25. Andreas, B. Energy efficiency-waste heat utilization with screw expanders. *Pumps Compress. Process Compon.* **2012**, 120–126.
26. Lemort, V.; Guillaume, L.; Legros, A.; Declaye, S.; Quoilin, S. A comparison of piston, screw and scroll expanders for small scale rankine cycle systems. In Proceedings of the 3rd International Conference on Microgeneration and Related Technologies, Napoli, Italy, 15–17 April 2013.
27. Moroz, L.; Kuo, C.R.; Guriev, O.; Li, Y.C. Axial turbine flow path design for an organic Rankine cycle using R-245fa. In Proceedings of the ASME Turbo Expo 2013, San Antonio, TX, USA, 3–7 June 2013.
28. Pasquale, D.; Ghidoni, A.; Rebay, S. Shape optimization of an organic Rankine cycle radial turbine nozzle. *J. Eng. Gas Turbines Power* **2013**, *135*, 042308:1–042308:13.
29. Yang, K.; Zhang, H.; Song, S.; Zhang, J.; Wu, Y.; Zhang, Y.; Wang, H.; Chang, Y.; Bei, C. Performance analysis of the vehicle diesel engine-ORC combined system based on a screw expander. *Energies* **2014**, *7*, 3400–3419.